Titanium Dioxide/Graphene Oxide Composite Coatings for 316 Stainless Steel Dental Implants

ABSTRACT

Stainless steel has been used in orthopedics and orthodontic fields. However, it cannot be used for fabrication of dental implants due to its inertness, low biocompatibility and weak resistance to corrosion. A composite coating of titanium oxide /graphene oxide has been prepared for stainless steel to improve its biological properties. Stainless steel discs were polished, cleaned and pre-treated with a mixture of HNO_3 and HF acid for 15 min. The composite coating composed of TiO_2 produced by sol-gel technique and doped with 0.75 wt% graphene oxide. XRD, SEM-EDX and AFM were employed to characterize the composite coating. The anti-bacterial action of the composite coating was investigated against S. aureus and E. coli. The corrosion resistance of coated and non-coated samples was assessed in SBF using electrochemical technique. Cytotoxicity was assessed using osteoblast-like cells. The wettability was determined by contact angle, and bioactivity assessed by immersion in SBF. The results revealed that the composite coating was dense with few micro-cracks, and was not cytotoxic to osteoblast-like cells. The composite coating reduced bacterial colonies and the corrosion rate of the steel was improved. The wettability of the sample was increased with the composite coating and apatite formation appeared after 21 days.

INTRODUCTION

Decade after decade, life expectancy increases and the demand for dental implants increases. Titanium and its alloy have been used to fabricate dental implants due to their suitable mechanical and biological properties. However, these materials are very expensive and difficult to manufacture and, therefore, have limited availability in more impoverished nations. Biomedical 316L stainless steel is currently used as an implant material in orthopedic and orthodontic fields due to its excellent mechanical properties (stiffness, ductility and elasticity), ease of production and low cost.[1,2] Therefore, such a metal may be useful to manufacture dental implants, especially in developing countries of low socioeconomic status. Practically, however, it is difficult to employ stainless steel dental implants due to its inertness,[3] low biocompatibility and low resistance to corrosion.[4] In addition to that, stainless steel implants are more prone to infection due to development of a fibrous fluid-filled capsule at the bone-implant interface that creates an ideal environment for bacterial colonization.[5] In order to overcome these shortcomings, several attempts have been conducted to modify the surface of stainless steel, particularly with thin or thick film

Keywords

Bioactivity
Titanium Dioxide
Coating, Corrosion
Graphene Oxide

Authors

Ahmed S. Al-Noaman *
(B.D.S, MSc., PhD)

Simon F. Rawlinson §
(BSc (Hons.), PhD)

Address for Correspondence

Ahmed S. Al-Noaman *

Email: aalnoaman7@gmail.com

* *University of Babylon, College of Dentistry, Department of Oral surgery, Babylon city, Iraq*

§ *Queen Mary University of London, School of Medicine and Dentistry, London, UK*

Received: 14.01.2023
Accepted: 21.03.2023

doi: 10.1922/EJPRD_2511Al-Noaman15

coatings and using different coating techniques. Among these techniques is the sol-gel method that has been used to coat stainless steel with bioactive materials such as hydroxyapatite,[6] bioactive glasses[7] and titanium dioxide.[8]

Titanium dioxide is a natural oxide of titanium. It occurs in amorphous and crystalline forms and produces three major crystalline phases: anatase, rutile and brookite; rutile and anatase have a tetragonal structure, while brookite is rhombic.[9] TiO_2 has excellent properties; biocompatible, bioactive and corrosion resistant. Further, the anatase, tetragonal configuration, has apatite forming ability in biological fluids.[10] More interestingly, this biomaterial has anti-microbial properties due to photo-catalyst activity.[11,12] It has been argued that TiO_2 exerts less antimicrobial activity in visible light and under dark conditions compared with the irradiated TiO_2.[13] However, the antibacterial action of this material might be not fully achieved in case of dental implants, as the implant fixture is situated inside bone and difficult to be activated by irradiation or visible light.

Normally, successfully osseo-integrated implants are embedded in bone, as long as the level of marginal bone is maintained. However, the supporting bone might be resorbed due to the remodeling process, thereby exposing implant surfaces. The exposed surfaces might become contaminated and any developing infection could lead to the loss of supporting tissues. Clinically, the biocidal effect of a TiO_2 coating in such a condition is questionable, because the photo-induced bactericidal effect is limited to the essential period for the implant to be accepted by the body.[14] The limited access to UV-light is another obstacle: it is difficult for the UV light to penetrate the surrounding thick tissues such as human gingiva and bone, and a further complication is that long-term or intense exposure to UV-light causes human tissue damage.[15] Therefore, to improve bactericidal effect of TiO_2 and to prevent biofilm formation and subsequent implant failure, a TiO_2 coating can be doped with graphene oxide. Graphene oxide has anti-bacterial action,[16] large surface area[17,18] and rich surface hydrophilic functional groups.[19]

In the present study, a TiO_2/graphene oxide composite coating was prepared by sol-gel dip coating technique to coat stainless steel in an attempt to improve its biological, resistance to corrosion and anti-bacterial properties.

MATERIALS AND METHODS

SUBSTRATE PREPARATION

16 mm diameter 316 medical grade stainless steel discs were degreased and manually polished with 180, 2000 and 3000 grits silica carbide Emery paper and diamond paste (Struers- 6 microns). The polished discs were rinsed in acetone and ethanol and left to dry at room temperature. Next the discs were pre-treated with a mixture of HNO_3:HF in a ratio 3:1 vol % for 15 min and washed with distilled water and left to dry at room temperature. The chemical composition of 316 medical grade stainless steel is shown in Table 1.

COATING PREPARATION

The TiO_2 sol was prepared by mixing poly (titanium IV butoxide) 97% ($CH_2CH_2CH_2CH_3$) (Jinan Boss chemicals) with distilled water, ethanol and HNO_3 in the molar ratio 1:1:37:0.1, as described elsewhere.[20] The mixture was left to stir vigorously for 2 h. For the composite coating, graphene oxide powder (Suzhou Tanfeng Graphene Technology) was mixed with distilled water for 1 h at room temperature. Then, about 0.75 wt% of the solution (100 µl) was added to the TiO_2 sol and stirred for 1 h. The composite coating was prepared by dip coating technique using PTL-MM01 dip coater (Zhengzhou Chuangda Laboratory Equipment Co., Ltd). The stainless steel substrate was soaked in the sol for 30 sec and withdrawn at a rate of 100 mm/sec. The coating cycle was repeated three times to obtain the desired coating thickness with the same soaking time and withdrawal speed. The coated samples were left to dry at room temperature for 24 h. Thereafter, the composite coating was subjected to heat treatment at 650 °C for 1 h and left in the muffle furnace to cool down.

COATING CHARACTERIZATION

Coated and non-coated stainless steel samples were characterized pre- and post-soaking in SBF by X-ray diffraction (XRD) (Dx2700AB) to probe the structure of the samples. The device was regulated at 50 kV/30 mA and copper (Cu) x-ray target at 2 theta range of 10-80° with a step size of 0.2/s. Scanning electron microscopy-energy dispersive spectroscopy (SEM-EDS) (S50.fei) was employed to evaluate the morphology of the surface coating, where the sample was mounted and point scan analysis performed to detect the elemental contents. The voltage power used in SEM imaging ranged between 10 and

Table 1. Chemical composition of medical grade 316L stainless steel (wt%)- (According to manufacturer certificate).

Fe	Cr	Ni	Mo	Cu	Co	Si	Al	Mn	V	P	S	C	N
Bal*	16.48	10.30	2.11	0.32	0.19	0.53	0.005	1.38	0.058	0.028	0.0006	0.021	0.023

Bal: Balance

15 kv. The sample was mounted in a vertical position to visualize the stainless steel coating interface and to measure the coating thickness. Atomic force microscopy (AFM, XE-NSOM), in contact mode, was employed to investigate the topography and surface roughness of the composite coating with a scan size of 5 µm X 5 µm.

EVALUATION OF ANTI-BACTERIAL ACTIVITY

The antibacterial action of pure TiO_2 and TiO_2/graphene oxide composite coatings was investigated against gram -ve *Escherichia coli* (*E. coli*) and gram +ve *Staphylococcus aureus (S. aureus)* bacteria counting colony forming units. The bacterial strains were gifted from the DNA center, University of Babylon. After centrifugation and turbidity adjustment to McFarland tube ($0.5*10^8$), about 150 µl of bacterial suspension in 0.9% NaCl was placed, drop wise on the sample surface contained in a (60*15 mm) polystyrene Petri-dish and covered with a lid for 3 h inside a sterile hood.[21] Then, brain heart broth media was added to cover the sample in the Petri-dish. About 200 µl of the surface contaminated bacterial suspension was added into a broth media to run a serial dilution up to 10^7. After that, 100 µl from each diluted broth culture media was inoculated into Muller-Hinton agar plate and incubated at 37 °C for 24 h. The number of viable bacterial colonies (CFU) was counted after incubation. The test was repeated three times for each sample. The log reduction of CFU/ml was calculated by subtraction of the minimum inhibition concentration from the McFarland concentration. Washed, polished, but uncoated stainless steel was used as a control.

CELL CULTURE

Human (osteosarcoma) osteoblast-like cells, MG-63, were used to assess cytotoxicity of the TiO_2/graphene oxide composite coating, using TiO_2 coating as the control. Cells were cultured in RPMI 1640 culture media (Sigma) containing 10% fetal bovine serum (Gibco, Grand Island) and 1% penicillin/streptomycin (Invitrogen, Grand Island) in a humidified incubator (5% CO2 at 37 °C). Confluent cells were separated using 0.25% trypsin (Sigma) and aliquots of detached cells were sub-cultured. Cells between the 7th – 14th passages were employed for the experiments.[22]

Human gingival fibroplast-1 (HGF-1), derive from gingival connective tissue, were also recruited to assess the cytotoxicity of the coated samples following the same technique of osteoblast-like cells.

IN VITRO CELL VIABILITY

For cytotoxicity assay, MG-63 osteoblast-like cells ($1x10^5$ cells/ml) were seeded onto the surface of sterilized coated samples in 24-well cell culture plates and incubated for 24 h at 37 °C, 5% CO_2. After exposure to the coated samples, 10 µl of MTT solution was added to each well. The plates were further incubated for 4 h. The media from each sample was carefully transferred to individual wells of a clean 24-well plate, 100 µl of dimethyl sulfoxide solubilization solution added and incubated for 5 min. Finally, the absorbance was measured using an ELISA reader (Bio-Rad) at 575 nm. The MTT assay was carried out at 24, 48 and 72 h time points according to the International Standard ISO 10993-part 5, 2009. The assay was repeated three times for each sample.

CORROSION PROPERTY OF THE COATED AND NON-COATED SAMPLES

The electrochemical test was carried out in a three-electrode cell containing simulated body fluid (SBF) for 15 min. using a computerized potentiostat (Wenking) with analyzing software. The reference and counter electrodes were Ag/AgCl and platinum. The non-coated and coated stainless steel were used as working electrodes. The SBF was prepared according to Kokubo method[23] using the chemical ingredients shown in Table 2. SBF was kept at 37 °C and a pH ranged between 7.4-7.8 to simulate the physiological condition of the body. The non-coated surface and the peripheries of the coated samples were wrapped with nitrocellulose which was used as an insulator during immersion in SBF. The polarization curves were measured between ±200 mV around the equilibrium potential at a rate of 0.5 mV/sec. The electrochemical test was carried out by measuring open circuit potential and the test was repeated three times for each sample. The corrosion rate (CR) was measured using the following equation:[24]

$$CR\ (mpy)=0.13\ (icorr.).(Ew)/A.p$$

Where 0.13 is a constant, *i*corr. is the electrical current (µA), Ew is the equivalent weight of the elements of stainless steel substrate (g/mol), A is the sample surface area subjected to electrochemical test (cm^2) and p is the density of stainless steel substrate which is ($7.8\ g/cm^3$).

Table 2. Electrochemical results of the bare stainless steel, stainless stelel coated with pure TiO_2 and TiO_2/GO compostie coatings in simulated body fluid.

Sample	Ecor (µV)	Icor (µA/nA)	CR (mpy)
Uncoated S.S.	-175.1	2.37	0.00543
S.S. coated with TiO_2	-173.6	0.363	0.000833
S.S. coated with TiO_2-GO	-155.2	0.796	0.00182

S.S.: Stainless steel

CONTACT ANGLE MEASUREMENT

The contact angle of a distilled water drop was measured using static drop method. Optical contact angle and interface tension meter (Kino) was employed to assess wettability of bare, TiO_2-coated and TiO_2-graphene oxide coated stainless steel samples. About 25 µL of distilled water was applied by micro-syringe and the contact angle was determined at three different points within 15 seconds after applying the drop using computer software.

APATITE MINERALIZATION

Deposition of surface apatite on TiO_2/graphene oxide composite coating and pure TiO_2 coatings was investigated with immersion in simulated body fluid (SBF) after 7, 14 and 21 days. The coated stainless steel discs were immersed in 20 ml SBF based on the surface area of the coated discs. The volume of SBF was determined using the following equation:[25]

$$Va = Sa/10$$

Where Va is the volume of solution (ml) and *Sa* is the surface area of the coated discs (mm^2).

The pH changes of the simulated body fluid were measured using a Pen Type pH Meter (pH-009 (I) A) at the prescribed time intervals. After taking the coated discs out from the incubator, they were left to dry at 37 °C.

STATISTICS

ANOVA (one way analysis of variance) and student-T test were used to determine any significant statistical differences. P value < 0.05 was considered statistically significant.

RESULTS

X- RAY DIFFRACTION

The XRD pattern of the composite coating reveals stainless steel diffraction peaks at 43.4 and 50.5 2Θ° (*Figure 1*). In addition to that, it exhibits crystalline peaks at 25, 37.5, 47.8, 53.7 and 54.8 2Θ° which pertained to (101, 004, 200, 105 and 211) crystalline planes of anatase-TiO_2 structure according to JCDP card no. 21-1272.[26] Notably, the crystalline peaks of graphene oxide at 10.54 2Θ° could not be seen in TiO_2/graphene oxide coating. Similar diffraction peaks have been seen in the XRD pattern of the pure TiO_2 coating (results not shown). Optically, the composite coating is transparent and the underlying stainless steel reflected through the composite coating.

SCANNING ELECTRON MICROSCOPY-ENERGY DISPERSIVE SPECTROSCOPY AND ATOMIC FORCE MICROSCOPY

Figure 2 shows SEM micrograph and EDX analysis of the pristine stainless steel. Grinding and polishing scratches could be seen, and there is no titanium in the chemical composition of the stainless steel. The micrographs reveal that the stainless steel surface is fully covered with the TiO_2/ graphene oxide composite coating and the coating is dense and uniform (*Figure 3A*). However, some micro-cracks, defects and white particles of different sizes were observed. The micro-cracks and defects seem to be filled with coating material due to repeating coating process. EDX analysis of the composite coating reveals the presence of Ti, C and O which indicate that the chemical composition of the composite coating contains TiO_2 and graphene oxide (*Figure 3B*). Notably, the highest weight ratio was assigned to O_2 of the composite coating.

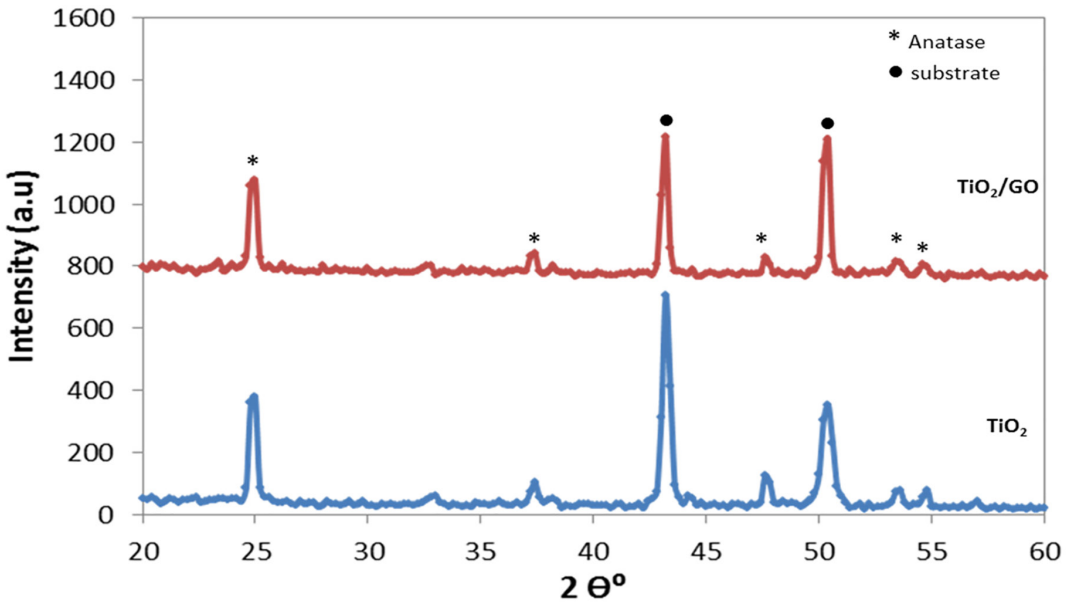

Figure 1: XRD analysis of titanium dioxide/graphene oxide composite coating and pure titanium dioxide coating. Anatase phase represents the main phase of titanium dioxide of both coatings. Both coatings exhibited similar diffraction peaks.

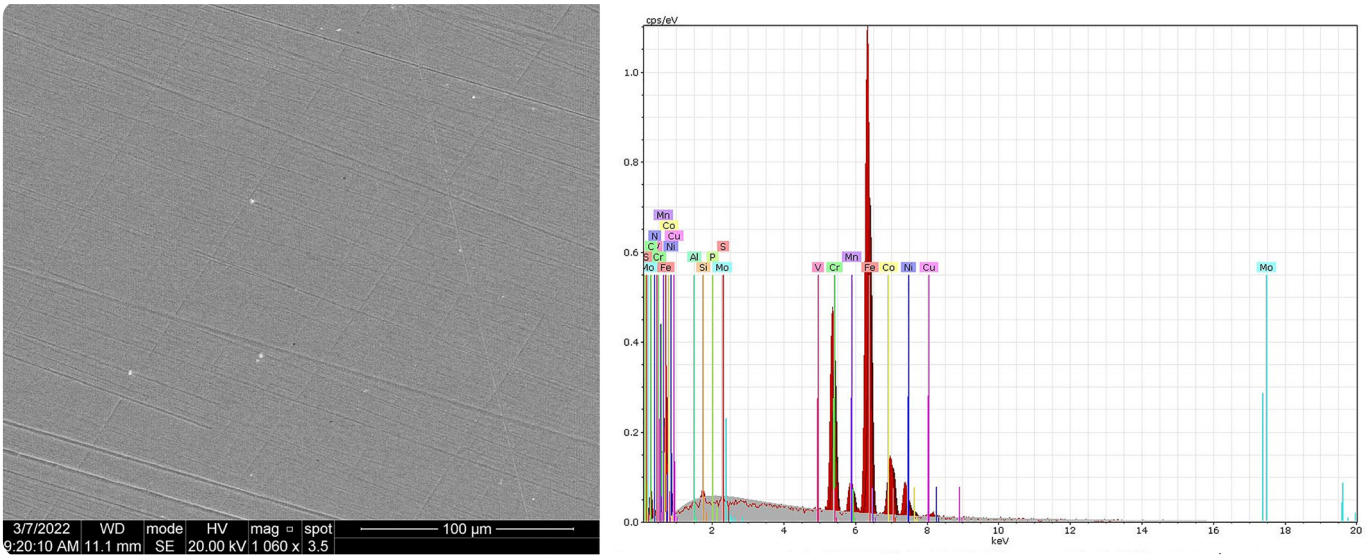

Figure 2: SEM micrograph and EDX analysis of the bare stainless steel showing grinding and polishing scratches and there is no titanium in the chemical composition of the bare stainless steel.

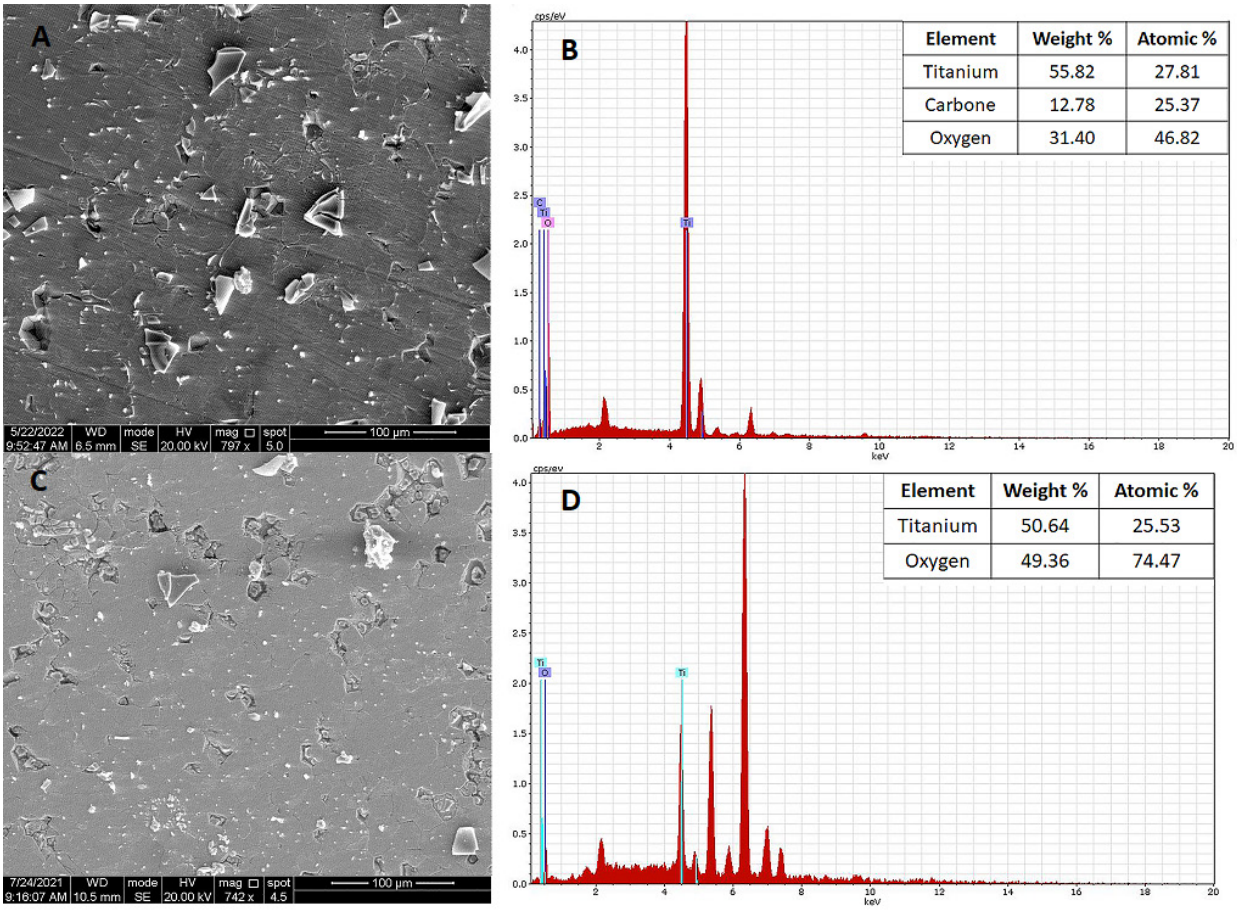

Figure 3: A) SEM- micrograph and B) EDX analysis of the titanium dioxide/graphene oxide composite coating. C) SEM-micrograph and D) EDX analysis of pure titanium dioxide coating. Defects and micro-cracks could be seen in the SEM-micrograph of the composite coating.

Figure 3C and D shows the SEM micrographs and EDX analysis of the pure TiO_2 coating. Similar features were observed in the SEM micrograph of the pure TiO_2 coating with more defects compared to that seen in the SEM micrograph of the composite coating. EDX analysis reveals Ti and O, which represent the chemical composition of the coating.

Figure 4A and B displays SEM micrograph of the composite coating/stainless steel interface and EDX analysis of the interface. The micrograph reveals that the coating is in close contact with the underlying substrate without micro-cracks or porosities. The visible thickness of the composite coating from the SEM micrograph is about 2.5 µm. EDX analysis of the interface

reveals elements such as Ti, O, C which represent the chemical composition of the composite coating. Interestingly, EDX analysis of the interface exhibited Fe and Cr at a higher concentrations which originate from the stainless steel substrate.

The AFM results (AFM 3D image and the value of the mean roughness, Ra) of the TiO_2/graphene oxide composite coating show that the coating surface is irregular, and the value of Ra is 34.7 nm, (*Figure 5*A). Greater surface irregularity with a higher Ra value (41.7 nm) were measured in the pure TiO_2 coating (*Figure 5*B). The bare stainless steel demonstrated the lowest Ra value (15.24 nm).

EVALUATION OF ANTI-BACTERIAL ACTIVITY

To simulate the environment of dental implant in the oral cavity, anti-microbial action of the composite coating was investigated in the dark. Figure 6 shows the results of anti-bacterial assay of the bare stainless steel, TiO_2/graphene oxide composite coating and TiO_2 coating against the studied bacteria. The results indicate that graphene oxide improved antimicrobial action of TiO_2 coating against gram +ve (*S. aureus*) and -ve bacteria (*E.coli*). The count of both bacterial species exposed to the composite coating reduced up to 99.99%. However, the antimicrobial effect of TiO_2/graphene oxide composite coating against *E. coli* was slightly greater than that against *S. aureus* with non-significant statistical differences ($p > 0.05$). The pure TiO_2 coating exhibited antimicrobial activity

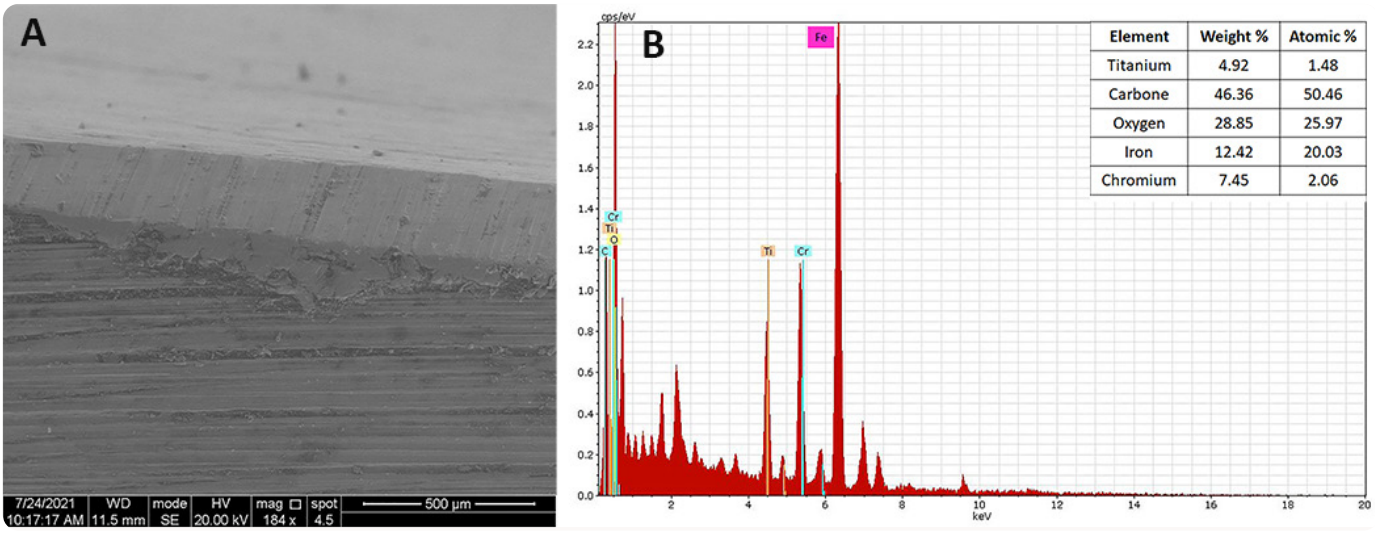

Figure 4: A) SEM- micrograph and B) EDX analysis of the titanium dioxide/graphene oxide composite coating- stainless steel interface. The visible thickness of the composite coating is 2.5 µm. There is no space or porosities between the composite coating and the stainless steel substrate indicating satisfactory adhesion between the two-phases. This was also approved by simple qualitative scratching test of the titanium dioxide/graphene oxide composite coating using dental probe. Presence of Cr in the EDX analysis of the interface indicates elemental diffusion between the two phases.

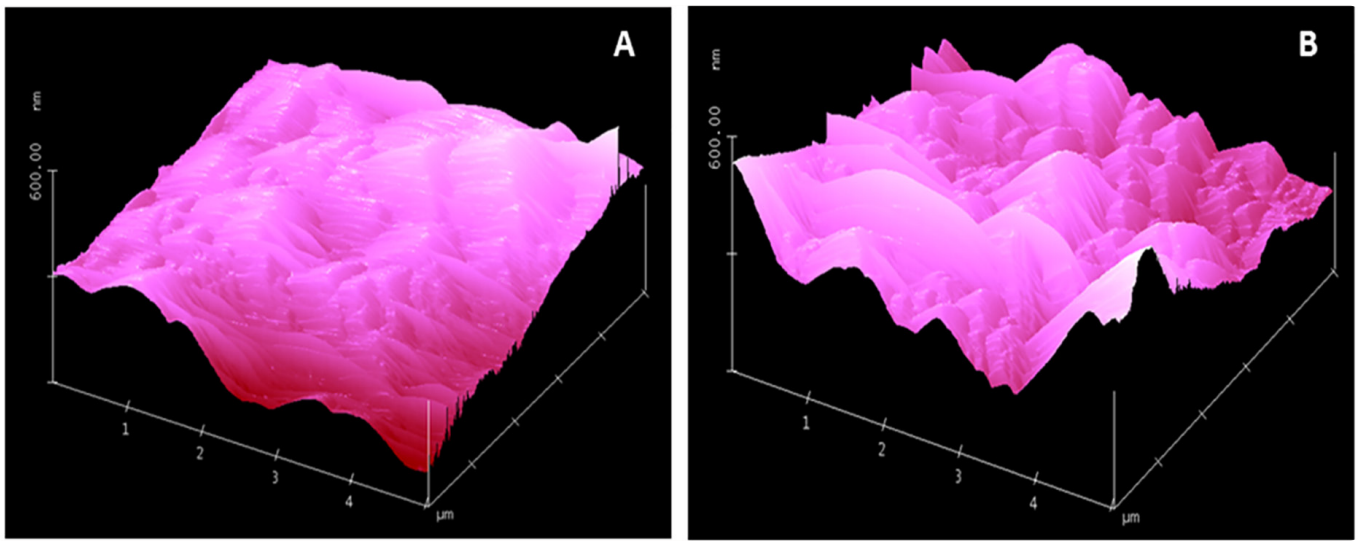

Figure 5: AFM analysis of A) titanium dioxide/graphene oxide composite coating and B) pure titanium dioxide at scan rate 5 µm X 5µm. Pure titanium dioxide coating demonstrates higher surface roughness compared with the composite coating.

against both bacterial species particularly *E. coli* but at lower percentage (99.9%) compared with that of the composite coating. Unexpectedly, the count of *E.coli* reduced to (99%) upon exposure to the bare stainless steel in the dark.

CONTACT ANGLE MEASUREMENT

Figure 7 illustrates the contact angle measurement of the bare stainless steel, TiO_2 and TiO_2/graphene oxide composite coatings. Both TiO_2 and TiO_2/graphene oxide coatings improved wettability of the stainless steel substrate. The contact angle of distilled water drop on the bare stainless steel decreased from 72° to 49° and 21° after coating with TiO_2 and TiO_2/graphene oxide coatings, respectively. The difference of the contact angle among the samples was statistically significant ($p < 0.0117$).

Interestingly, there is only a weak inverse correlation (R^2=0.446) between the contact angle and the surface roughness of the bare stainless steel and the coated samples (TiO_2/graphene oxide composite coating and the pure TiO_2 coating).

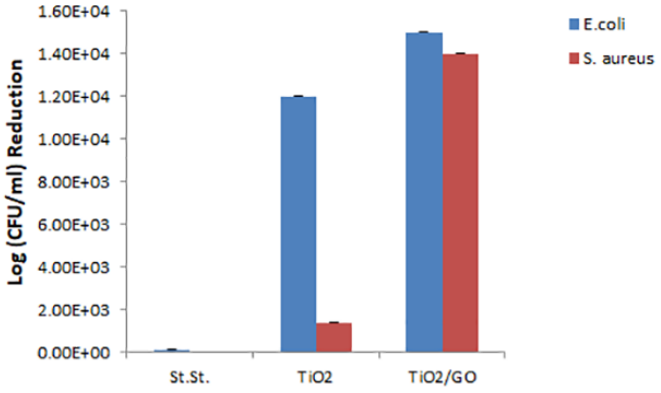

Figure 6: Anti-bacterial action of titanium dioxide/graphene oxide composite coating against *S. aureus* and *E. coli*. Titanium dioxide/graphene oxide exhibited higher anti-bacterial activity against both bacterial strains compared with pure titanium dioxide coating.

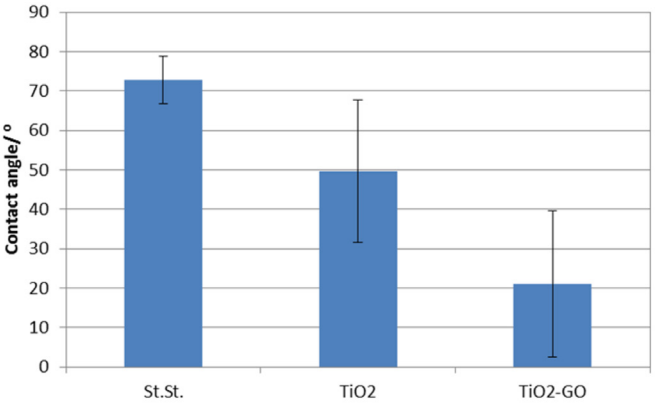

Figure 7: Contact angle measurement of the bare stainless steel, pure titanium dioxide coating and titanium dioxide/graphene oxide composite coating. Titanium dioxide/graphene oxide composite coating demonstrates lowest contact angle among other samples.

IN VITRO CELL VIABILITY

The number of viable MG-63 cells adhered to the TiO_2/graphene oxide composite coating was slightly higher (although, non-significant) than that of the pure TiO_2 coating in the first 24 h (91.67% vs. 91.59%, respectively) *(Figure 8A)*. The number of the attached cells on both coatings decreased steadily after 48 and 72 h, the composite coating still demonstrated slightly higher number of attached cells than those attached to the pure TiO_2 coating (86.27% and 80.02% vs. 83.03% and 79.55%, respectively). However, there were non-significant statistical differences in the number of the attached cells to the composite coating and the pure TiO_2 coating after 48 and 72 h.

Similar results were found for the primary human gingival fibroblasts *(Figure 8B)* - non-significant statistical differences of cell attachment to the composite and the pure TiO_2 coating in the first 24 h (93.48% vs. 94.52%). The number of the attached cells on the composite coating and the pure TiO_2 coating decreased gradually to (90.90% and 91.13%) after 48 h with non-significant statistical differences. After 72 h, the decrease continued (79.59% vs. 85.15%) with a significant statistical difference ($p < 0.0052$).

CORROSION PROPERTY OF THE COATED AND NON-COATED SAMPLES

Table 3 illustrates the results of electrochemical assay of the coated and bare stainless steel in the simulated body fluid for 15 min. The corrosive potential (E_{corr}) and corrosive current (I_{corr}) were obtained from the polarization curves using Tafel fit, as shown in Figure 9. The results revealed that TiO_2/graphene oxide composite coating increases the corrosion potential (E_{corr}) i.e to a less negative value (-155.2 mV) and reduces the consumption of the corrosive current (Icorr) to nanometer levels (796.79 nA) of the stainless steel substrate; the corrosion rate of the bare stainless steel also has been improved when coated with the composite coating. However, the pure TiO_2 coating improved the corrosion rate of the stainless steel substrate more than that of the TiO_2/ graphene oxide composite coating (84% vs. 66%, respectively) and decreases the consumption of the corrosive current (0.363 nA). Figure 9 and Table 3

APATITE MINERALIZATION

X- ray diffraction

The XRD pattern of the composite coating after 7 days immersion in the SBF showed new diffraction peaks at 10.6, 21.8 and 45.4 2Θ° *(Figure 10)* which correspond to 100, 200 and 203 of hydroxyapatite planes.[27] However, the main diffraction peaks of hydroxyapatite at 31.6 - 32 2Θ° could not be seen. After 14 days immersion, a broad and ill-defined diffraction peak was beginning to emerge.[28] The main diffraction peaks of hydroxyapatite appears very clear as a single sharp and narrow peak at 31.6 2Θ° after 21 days immersion in the SBF. The

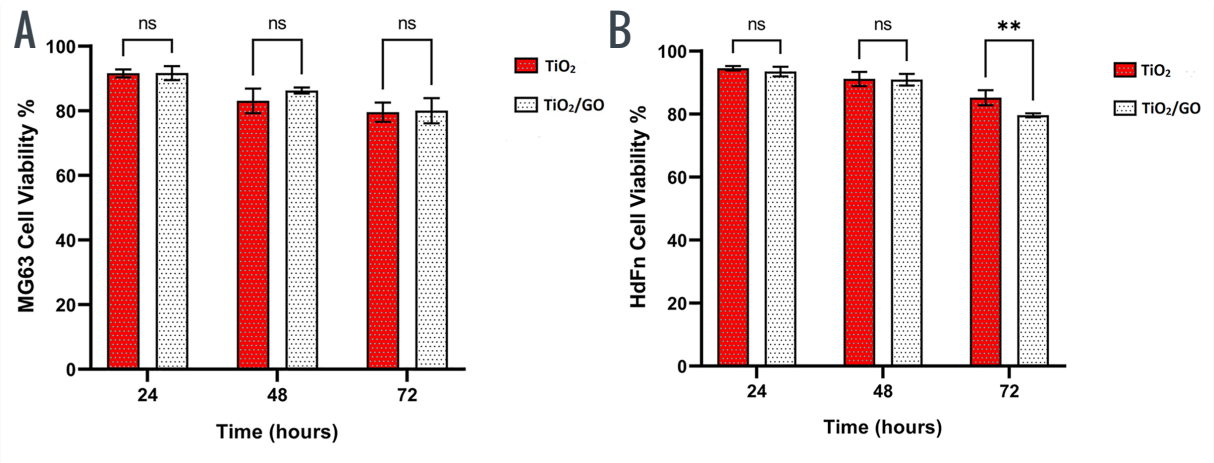

Figure 8: Cytotoxicity assay of titanium dioxide/graphene oxide composite coating against A) osteoblast-like cells and B) fibroblast cells. After 72 h, the count of osteoblast-like cells and fibroblasts within 80% indicates biocompatibility of the composite coating.

Table 3. Chemical composition of simulated body fluid g/l (green) and mmol (clear).

NaCl	$NaHCO_3$	KCl	$K_2HPO_{4.2}H_2O$	$MgCl_2.6H_2O$	$CaCl_2.2H_20$	Na_2SO_4	$(CH_2OH)_3CNH_2$	HCl
6.546	2.268	0.373	0.178	0.305	0.368	0.071	6.057	40
112.00	26.99	5.00	0.84	1.50	2.50	0.49	50.00	2.3

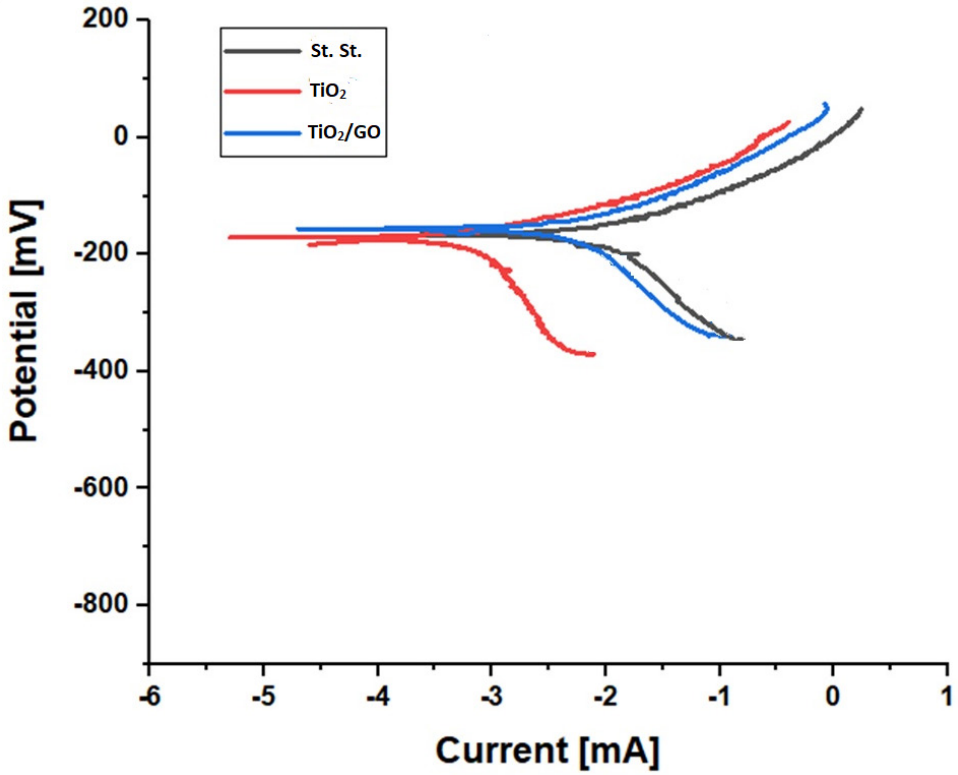

Figure 9: Potentiodynamic polarization curves for the bare stainless steel and coated samples in a simulated body fluid (SBF). Titanium dioxide/graphene oxide composite coating increases corrosion potential (E_{corr}) and reduces the consumption of corrosive current (I_{corr}).

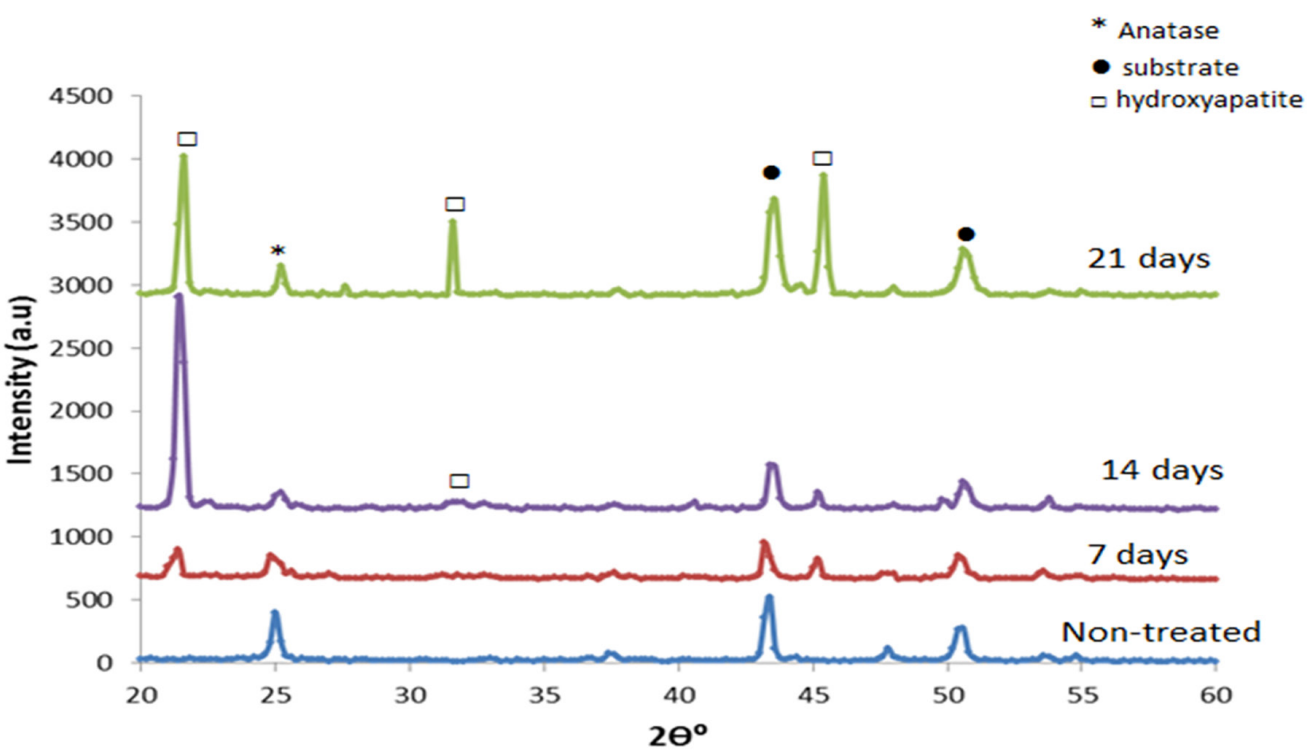

Figure 10: XRD analysis of not- treated and treated titanium dioxide/graphene oxide composite coating in simulated body fluid after 7, 14 and 21 days. Low intensity and broad peak of hydroxyapatite appears after 14 days immersion in simulated body fluid at 31.8 2Θ°.

diffraction peaks of anatase-TiO_2 and the stainless steel are visible in the XRD pattern of the composite coating. Similar diffraction peaks of less intensity were seen in the XRD pattern of the pure TiO_2 coating after the same time intervals of immersion in the SBF (results not shown).

Scanning electron microscopy-energy dispersive spectroscopy

Single agglomerates distributed randomly over the surface of the composite coating were detectable after 21 days immersion in the SBF *(Figure 11A*). EDX analysis of these agglomerates presents the main elements of bone hydroxyapatite i.e Ca and P *(Figure 11B*). The atomic ratio of Ca to P of these agglomerates was 1.2. SEM micrographs of the composite coating after 7 and 14 days soaking demonstrates little, if any agglomerates compared with that observed after 21 days immersion (data not shown). SEM micrograph of the pure TiO_2 coating demonstrates few isolated agglomerates after 21 days immersion in the SBF, and the Ca: P ratio obtained from EDX analysis was 0.4 which reveals a phosphorus-rich phase of the observed appetite agglomerates on the pure TiO_2 coating *(Figure 11C and D)*.

DISCUSSION

Studies have been undertaken to assess the osteogenic potential of titanium dioxide[29] and graphene oxide[30] as a coating for titanium-based dental implants to improve bone-implant integration. However, other properties such as bioactivity, corrosion resistance and anti-microbial action to improve the life of dental implants have rarely been considered. In this study, the effect of these biomaterials in combination has been employed to evaluate biological, antimicrobial and corrosion resistance for use with stainless steel-based dental implants.

COATING CHARACTERIZATION

The diffraction peaks of stainless steel and those of anatase-TiO_2 observed in the XRD pattern of the TiO_2/graphene oxide composite coating and TiO_2 coating are consistent with earlier studies.[8,26,31] Further, the similarity in the intensities of the peak crystallization of both coatings indicate that doping graphene oxide at 0.75 wt% did not affect the crystallization process of anatase. This is obvious from the absence of the main diffraction peak of graphene oxide at 10.54 2Θ° in the XRD pattern of TiO_2/graphene oxide composite coating. The absence of the main diffraction peak of graphene oxide could be either due to destruction of the regular stack of graphene oxide as a result of the intercalation of TiO_2 particles;[32] or due to the low amount of graphene oxide doped into the TiO_2 sol which is below the detection capacity of the diffractometer. These findings are consistent with study of [33] where graphene oxide was added to TiO_2 coating at a mass ratio 15:8, but the main diffraction peak could not be seen.

The micro-cracks and defects observed in the SEM micrograph of the composite coating may occur during drying process due to stress and tension forces of the liquid inside the pores of the drying body;[34] or due to thermal expansion mismatch between the stainless steel and the composite coating (17x10-6 and 2.1-2.8x10-6 / °C, respectively)[35] during cooling

ejprd.org - Published by Dennis Barber Journals.

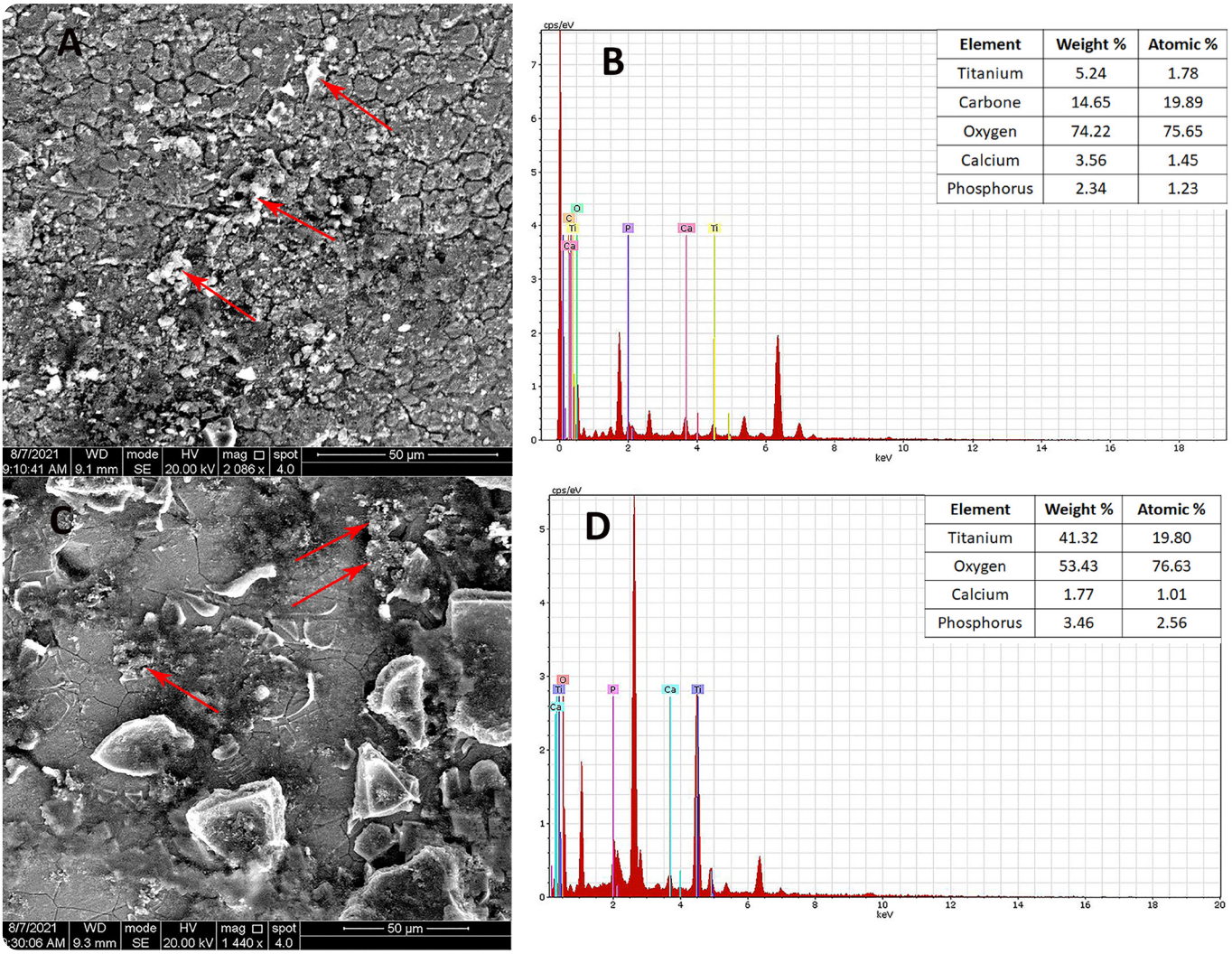

Figure 11: A & C) SEM-micrograph and EDX analysis of the titanium dioxide/graphene oxide composite coating and B & D) SEM- micrograph and EDX analysis of the pure titanium dioxide coating after 21 days immersion in simulated body fluid. Red arrows indicate randomly distributed hydroxyapatite agglomerates on the composite coating and phosphorus-rich apatite on pure titanium dioxide coating.

of the annealed films.[36,37] According to the EDX spectrum, the observed white particles are anatase-TiO_2 crystals that formed during firing process. Similar features have been observed in the SEM-micrograph of the TiO_2 coating with fewer white particles. The EDX spectra of the TiO_2/graphene oxide composite coating showed that Ti, O and C elements distributed evenly, indicating homogeneity of the composite coating. Further, the high weight ratio of O_2 is because this element is present in both TiO_2 and graphene oxide. EDX-analysis of the pure TiO_2 coating shows only Ti and O, indicating that this coating is devoid of the carbon containing graphene oxide.

SEM micrographs of the coating/stainless steel interface indicate that the coating adheres to the underlying substrate and the micro-cracks seen in the coating surface do not involve the entire coating thickness. This is probably due to repeating the coating cycles. The thickness of the composite coating synthesized in this study where three dip coating cycles had been used is more than that produced in the study of [38] (2.5 µm vs. 0.412 nm). These differences in the coating thickness could be due to the different parameters used during dip-coating technique. The study of [38] used a rate was 220 mm/min and the deposited layer was dried at 200 °C for 5 min in a furnace after each dip-coating cycle. The existence of Fe and Cr in the EDX analysis of the interface is associated with a high concentration of these elements in the chemical composition of the underlying stainless steel substrate.

The composite coating is irregular with mean surface roughness 34.7 nm and could be because of the crystalline particles of the anatase-TiO_2 coating and graphene oxide particles doped into TiO_2 sol during coating preparation. In addition to that, the presence of pores and defects of the composite coating could be a further reason for the surface roughness. However, the mean Ra of the pure TiO_2 coating is higher (41.7 nm) than that of the composite coating, which could be because of the grain boundary of TiO_2 grains 39 or defects of the pure TiO_2 coating. This difference between the composite and the pure TiO_2 coatings is because of graphene oxide. Doping graphene oxide into the pure TiO_2 coating smooths the coating surface by overlapping the TiO_2 grain boundary. One of the prerequisites for successful dental implantation is a high surface roughness; as it provides a large surface area, promotes friction, improves osseo-integration and supports early implant stability.[40]

It has been reported that graphene oxide has antimicrobial activity against gram +ve and -ve bacteria.[41] Therefore, doping graphene oxide into a TiO_2 matrix would be expected to improve the antimicrobial action of the composite coating. Although, *E. coli* was more affected by the anti-bacterial action of the composite coating compared with *S. aureus*, there were non-significant statistical differences between the two bacterial strains. To explain the mechanism of anti-bacterial action of graphene oxide; Lui *et al*.[42] proposed that the sharp edges of graphene oxide disrupt the cell membrane of *E. coli*. Others stated that graphene oxide damaged bacterial cells by production of reactive oxygen species (ROSs)[43]; phospholipid extraction[44] and intertwining[45,46] are other explanations for the bactericidal effect of graphene oxide.

The pure TiO_2 coating exhibited lower antibacterial activity against the studied bacterial strains in the dark (99.9%) with a more intense effect on *E. coli* compared with *S. aureus*. These findings confirm that doping graphene oxide into TiO_2 matrix improved the anti-bacterial action of the latter against the tested bacteria. The results of the pure TiO_2 coating are in agreement with other studies[47,48] where they explained the reduction in the count of bacterial cells in the dark to the decrease of the pH due to addition of the photo-catalysts. However, other studies ascribed the anti-bacterial activity to the ability of TiO_2 to inhibit bacterial adhesion through altering surface free energy of the coated surfaces[49] or increasing electron donor surface energy of the coating.[50,51] Further, Babaei *et al*.[52] attributed the decrease in the number of the adhered bacterial strains to the intense bonds of the positively free titanium ions in the media with the negatively outer layer of the bacterial cell wall which increases slipping of *E. coli* and *S. aureus* in the culture media.

The findings of the antimicrobial assay revealed that *E. coli* was more affected by the bactericidal effect of TiO_2/graphene oxide composite and the pure TiO_2 coatings compared with *S. aureus*. *E. coli* has thin cell membrane with loose poly-saccharide layer of 10 nm which can be destructed physically by the nano-sharp edge of graphene oxide; whereas, *S. aureus* surrounded by a dense with thick poly-saccharide layer of 20-80 nm that protects them from the harmful effect of graphene oxide.[53] In addition to that, anaerobic bacteria such as *E. coli* are more sensitive to O_2 tension compared with aerobic bacteria.[54] The abundant O_2 from graphene oxide functional groups and TiO_2, as demonstrated in the EDX analysis of the TiO_2/graphene oxide composite coating, generate more O_2 tension which are unfavorable for survival of *E. coli*. Lastly, the potential antibacterial activity of both coatings against *E. coli* could be ascribed to the positively charged free metal ions released from the TiO_2 coating in the media which react with lipids through the negatively charged bacterium cell wall; the binding of the TiO_2 particles with the cell wall affects membrane fluidity which causes decomposition of the phospholipids, decreases its hydrophobic properties and eventually leads to bacterial death.[55] The graphene oxide used in this study has a multi-layered structure; therefore, the suggested mechanism of anti-bacterial action of the TiO_2/graphene oxide composite coating was due to physical destruction rather than the generation of ROSs.

The reduction in *E. coli* counts exposed to the bare stainless steel could be related to the polished and smooth stainless steel surfaces and the size and form of the bacteria which affect the area of bacteria-surface contact.[56] It has been shown that *E. coli* requires greater surface roughness (large cavities) to adhere to 316 stainless steel surfaces due to its rod-like shape; whereas, small spherical shape *S. aureus* adheres faster and requires lower levels of surface roughness to attach to stainless steel surfaces.[57] Besides, this reduction in the number of viable bacteria could be associated with the chromium oxide IV formed on the stainless steel substrate which has a toxic effect and structural damage to the studied bacteria.[58]

The increased wettability of stainless steel after coating with TiO_2 coating is due to the hydrophilic nature of this compound; as TiO_2, like other metal oxides, has a high surface energy and hence is highly hydrophilic, providing that its surface is free of contamination.[59] It was found that, compared to the films containing rutile, the anatase films retained high hydrophilicity due to the formation of strong donor-acceptor complexes by the interaction of Ti-OH basic groups with H_2O.[60] This implies that the anatase-TiO_2 rich surface will be dominantly hydrophilic and inherently more so compared with the rutile films.[61] Further increases in the wettability of the stainless steel after coating with TiO_2/graphene oxide composite coating is because of the abundant hydrophilic functional groups present on the surface of graphene oxide[62] doped into the TiO_2 matrix. Increased hydrophilicity is important for bioactivity of the implant surface and to ensure biocompatibility and promote the early stages of osseo-integration by affecting cellular growth and accelerating the adhesion of plasma proteins.[63,64]

The surface roughness of the TiO_2/graphene oxide composite coating was slightly lower than that of the pure TiO_2 coating (34.7 vs. 41.7 nm); but demonstrated better hydrophilicity compared with the pure TiO_2 coating (contact angle- 21 vs. 49°). The decrease in surface roughness of the TiO_2/graphene oxide composite coating after addition of graphene oxide could be associated with the structure of graphene oxide, as it is multi-layered (according to manufacturer certificate). It has been argued that roughness measurement of graphene film decreases with an increase in layers.[65]. However, the low concentration of graphene oxide (0.75 wt%) could be another reason behind the decrease in the surface roughness of the composite coating. Graphene oxide at this concentration improved hydrophilicity of the TiO_2/ GO composite coating and it has been claimed that even small amounts of graphene oxide could improve hydrophilicity of the composite material.[66] Similar findings have been observed by Cao *et al*.,[67] where graphene oxide-loaded titanium nano-tubes (TNT-GO) modified Ti surfaces exhibited slightly lower surface roughness and higher hydrophilicity compared with titanium nanotubes (TNT) (42.1 vs. 46.5 nm) and (33.9° vs. 46°), respectively.

It was expected that the composite coating would exhibit greater numbers of attached viable cells compared to the TiO_2 coating, as the composite coating contains graphene oxide which increases the surface area and hydrophilicity of the composite coating. However, the results showed that the differences were not statistically significant after 24 h. This could be due to the low levels of graphene oxide (0.75 wt%) doped into TiO_2 sol which supported by the XRD analysis, as no graphene oxide diffraction peak was seen in the XRD pattern of the composite coating. In addition to that, the hydrophilic nature of the pure TiO_2 coating facilitates the adhesion and proliferation of eukaryotic cells.[68]

After 48 and 72 h, the number of viable cells attached to both coatings decreased gradually but the composite coating still exhibited higher numbers compared with the pure TiO_2 coating. This could be attributed to the relative increase in the surface area of the composite coating due to doping graphene oxide into the pure TiO_2 sol. The decrease in the number of viable cells on both coatings could be due to exhaustion of the culture media.

The XRD analysis of the TiO_2/graphene oxide composite coating and the TiO_2 coating showed that the main diffraction phase was anatase-TiO_2 after annealing at 650 °C. The findings of this study disagree with the study of 69 where they found that anatase-TiO_2 obtained from sintering TiO_2 powder at 700 °C suppressed the growth and proliferation of mouse osteoblast-like cells. However, the proliferation and growth of the Chinese Hamster ovary cells seeded on anatase-TiO_2 thin film obtained by magnetron sputtering technique were increased after 48 and 72 h.[70] These differences in the studies could be assigned to the type of cell-line used and the method employed for coating fabrication.

The behavior of primary human fibroblasts after 24 and 48 h were similar to that of the osteoblast-like cells. However, the composite coating had fewer viable cells after 72 h compared with the pure TiO_2 coating which could be related to experimental errors. The number of viable cells observed on the composite coating is still within viability 79.59%, and these findings indicate that the TiO_2/graphene oxide composite coating is a biocompatible material according to ISO 10993-5 8; i.e the viability is more than 70%, and could be considered as a coating for dental implants.

The increase in corrosion potential and the decrease of the corrosive current of the bare stainless steel is due to the TiO_2/graphene oxide composite coating and the pure TiO_2 coating. This effect is mainly related to the titanium dioxide matrix which has excellent corrosive resistance due to its ceramic protective barrier on the metal surface.[71] In addition to that, titanium dioxide is an inorganic compound and its inertness in the corrosive media decreases the substrate dissolution rate in the biological fluids.[72] Titanium dioxide reduces the substrate dissolution rate by preventing ionic release from the bare stainless steel into the solution and resisting the aggressive attack of the ions in the SBF.[73] However, stainless steel coated with the pure TiO_2 coating exhibited a lower corrosive current and higher corrosion rate compared with that of the composite coating. This is because the presence of oxygen functional groups on the basal plane of graphene oxide in the TiO_2 coating increases hydrophilicity of the composite coating which promotes absorption and diffusion of the solution molecules.[74] Therefore, the consumption of the corrosive current decreases and resistance to corrosion of the bare stainless steel improves by the composite coating but to a lower extent compared with the pure TiO_2 coating (66% vs. 84%).

APATITE MINERALIZATION

The existance of new diffraction peaks in the XRD pattern of the TiO_2/graphene oxide composite coating after 7 days soaking denotes that surface apatite began to form. This is ascribed to the anatase phase which is the dominant phase as discussed previously. Previous research stated that this phase has a similar hexagonal structure to that of HA crystal;[10] and the Ti-OH groups present on the surface of the TiO_2-anatase phase promote the formation of surface apatite.[76,77] However, the main diffraction peak of hydroxyapatite could not be observed after 7 days immersion. After 14 days immersion, a broad, but not-well defined, diffraction peak appears at 31.6 2Θ° which is associated with small size or low amount of crystal apatite formation.[78] The growth of this apatite was reflected in the XRD pattern of the composite coating after 21 days soaking as the main diffraction peak appears to be sharp and narrow which is associated with high crystallinity or large size apatite.[78] Previous studies have concluded that TiO_2 sol- gel dip coating annealed at > 600 °C may reduce the number of OH groups present on the TiO_2 surfaces[10] and this may retard apatite formation in the biological fluids. In this study, the TiO_2/graphene oxide composite coating was subjected to 650 °C for 1 h to obtain the anatase phase and this could explain the delay in apatite formation.

SEM micrographs of the composite coating also revealed the presence of agglomerates of apatite forming at 21 days of immersion in the SBF. However, these agglomerates were distributed randomly, and the surface of the composite coating was not completely covered. The apatite deposited on the anatase-TiO_2 phase - the main phase of the composite coating according to the XRD results. It has been proposed that anatase-TiO_2 can form bone-like apatite due to the crystallographic similarity between apatite (0001) plane and anatase (110) plane.[10] Further, anatase phase is rich in Ti-OH groups and large numbers of such groups are essential for apatite nucleation.[76,77] Others have stated that the bioactivity of anatase phase is related to its ability to absorb OH- and $PO4^{-3}$ from the biological fluid[79,80] and the presence of OH functional groups is imperative to enhance nucleation of calcium-phosphate.[81] However, the high temperature used during annealing process at 650 °C reduces the OH groups through dehydration and poly-condensation.[10] In addition, such temperatures may reduce the surface area of the coating due to a decrease in the pore size inherited from the sol-gel methods.[82] All these factors explain the longer time required for apatite deposition

or low amount of apatite formed on the composite coating. Apparently, the delay in apatite nucleation and deposition on the composite coating is not only associated with the annealing process, but also with the coating technique. The coating produced by sol-gel technique is usually thin and has low degradation rate i.e chemically stable.[83]

The Ca:P molar ratio of 1.2 of the apatite formed on the surface of the composite coating indicates that calcium-deficient apatite was formed.[84] This low Ca:P ratio could be related to the high affinity of TiO_2 to $HPO4^{-3}$ present in the SBF at the expense of Ca^{+2} [85] or to the carbonate, or hydrogen phosphate substitution for phosphate in the apatite structure.[86]

The low Ca:P ratio of calcium-deficient hydroxyapatite increases its solubility and bioactivity compared with stoichiometric hydroxyapatite.[87,88] It has been proposed that calcium-deficient hydroxyapatite is more advantageous for bone regeneration, as its composition and structure is close to that of natural bone minerals.[89]

SEM micrograph of the pure TiO_2 coating displays few isolated agglomerates distributed all over the coating surface. This feature and the low and weak intensities diffraction peaks seen in the pure TiO_2 coating after immersion in the SBF indicates low bioactivity of the pure TiO_2 coating compared with the composite coating. The low bioactivity of the pure TiO_2 coating could be attributed to the weak capability of the pure TiO_2 coating to adsorb Ca and P from the SBF due to low wettability of this coating as some organic groups adhered to the TiO_2 gel prepared by hydrolysis of titanium precursors.[20] EDX analysis of the observed agglomerates revealed that P was evenly distributed whereas Ca found only close to apatite agglomerates. The Ca:P ratio obtained from the EDX analysis is different from that of the stoichiometric apatite (1.67) and suggests the presence of phosphate-rich phase apatite which is also explained by the high affinity of TiO_2 to HPO_4^{-3} compared with Ca^{+2} in the SBF.

The differences in bioactivity of the composite and pure TiO_2 coatings could be related to the presence of graphene oxide, as this compound increases the wettability of the composite coating as explained previously. Therefore, the composite coating exhibited better apatite formation compared with the pure TiO_2 coating.

CONCLUSION

This study was carried out to evaluate the effect of TiO_2/graphene oxide composite coating on bioactivity, antimicrobial and anticorrosive properties of stainless steel dental implant. TiO_2/graphene oxide composite coating is dense, rough and transparent with few micro-cracks and defects. The anti-bacterial action of the TiO_2 coating was improved by doping graphene oxide and was more pronounced on gram –ve bacteria than gram +ve one. The coating was not cytotoxic at 0.75 wt% graphene oxide concentration to osteoblast-like cells and fibroblast cells. The composite coating improved wettability, reduced the corrosion rate of the stainless steel and demonstrate calcium-deficient hydroxyapatite formation after 21 days immersion in simulated body fluid. Given the prohibitive costs of titanium implants to some, the modification of stainless steel with a TiO_2/graphene oxide composite coating might provide the opportunity of more affordable dental care.

REFERENCES

1. Chauhan, P., Koul, V. and Bhatnagar, N. Design and Development of Indigenous Dental Implant System: From Research to Reality. *Trends Biomater. Artif. Organs.* 2018; **32**:51-61.
2. Mohandoss, S., Ganeasan, M.S., Manovasuki, J. and Sridhar, T. Surface Modification of 316L Stainless Steel Dental Implants by Novel Bioinert Nano Zirconia Coating. *Trends Biomater. Artif. Organs.* 2020; **34**:100-107.
3. Ashtiani, E.R., Alam, M, Tavakolizadeh, S. and Abbasi, K. The Role of Biomaterials and Biocompatible Materials in Implant-Supported Dental Prosthesis. *Evid Based Complement Alternat Med.* 2021;**2021**:3349433.
4. Oliver, J.N., Su, Y., Lu, X., Kuo, P.H., Du, J. and Zhu, D. Bioactive glass coatings on metallic implants for biomedical applications. *Bioact Mater.* 2019; **5**:261-270.
5. Stewart, S., Bryant, S.J., Ahn, J. and Hankenson, K.D. *Bone Regeneration.* 2015;313-333.
6. Kaur, S., Bala, N. and Khosla, C. Characterization of hydroxyapatite coating on 316 stainless steel by sol-gel technique. *Surf. Eng. Appl. Electrochem.* 2019; **55**:357-366.
7. Nivedha, V. and Ballamurugan, A.M. Sol–gel derived biologically relevant ions substituted bioglass coating on 316L stainless steel substrate for its anti-bacterial and corrosion resistance behavior. *J Sol-Gel Sci Technol.* 2017; **84**:323–331.
8. Burnat, B., Olejarz, P., Batory, D., Cichomski, M., Kaminska, M. and Bociaga, D. Titanium Dioxide Coatings Doubly-Doped with Ca and Ag Ions as Corrosion Resistant, Biocompatible, and Bioactive Materials for Medical Applications. *Coatings.* 2020; **10**:169.
9. De Dicastillo, C. L., Correa, M. G., Martínez, F. B., Streitt, C. and Galotto, M.J. *Antimicrobial Effect of Titanium Dioxide Nanoparticles.* In: Mareș, M., Lim, S. H. E. , Lai, K. , Cristina, R. , editors. Antimicrobial Resistance - A One Health Perspective. London: Intech Open, 2020.
10. Uchida, M., Kim, H.M., Kokubo, T., Fujibayashi, S. and Nakamura, T. Structural dependence of apatite formation on titania gels in a simulated body fluid. *J Biomed Mater Res A.* 2003; **64**:164-170.
11. Jo, W-K., Kumar, S., Isaacs, M.A., Lee, A.F. and Karthikeyan, S. Cobalt promoted TiO_2/graphene oxide for the photocatalytic degradation of oxytetracycline and Congo Red. *Appl. Catal. B: Environmental.* 2017; **201**:159-168.
12. Peng, G., Li, A., Sun, D.D. and Ng, W.J. Effects of various TiO_2 nanostructures and graphene oxide on photocatalytic activity of TiO_2. *J Hazard Mater.* 2014; **279**:96-104.
13. Kangwansupamonkon, W., Lauruengtana, V., Surassmo, S. and Ruktanonchai, U. Antibacterial effect of apatite-coated titanium dioxide for textiles applications. Nanomedicine: Nanomed.: *Nanotechnol. Biol. Med.* 2009; **5**:240-249.
14. Kumaravel, V., Nair, K.M., Mathew, S., Bartlett, J., Kennedy, J.E., Manning, H.G., Whelan, B.J., Leyland, N.S. and Pillai, S.C. Antimicrobial TiO_2 nanocomposite coatings for surfaces, dental and orthopaedic implants. *Chem Eng J.* 2021; **416**:129071.

ejprd.org - Published by Dennis Barber Journals.

15. Suketa, N., Sawase, T., Kitaura, H., Naito, M., Baba, K., Nakayama, K., Wennerberg, A. and Atsuta, M. An antibacterial surface on dental implants, based on the photocatalytic bactericidal effect. *Clin Implant Dent Relat Res.* 2005; **7**:105-111.
16. Shih, S.J., Chen, C.Y., Lin, Y.C., Lee, J.C. and Ren-Jei Chung, R.J. Investigation of bioactive and antibacterial effects of graphene oxide-doped bioactive glass. *Adv Powder Technol.* 2016; **27**:1013-1020.
17. Deng, Q., Chen, C., Lei, Q., Liang, J., Zhang, T. and Jiang, J. Adsorption of aniline from aqueous solution using graphene oxide-modified attapulgite composites. *RSC Adv.* 2018; **8**:23382-23389.
18. Wang, J., Liu, R. and Yin, X. Adsorptive Removal of Tetracycline on Graphene Oxide Loaded with Titanium Dioxide Composites and Photocatalytic Regeneration of the Adsorbents. *J. Chem. Eng.*, 2018; **63**:409–416.
19. Yoon, Y., Kye, H., Yang, W.S. and Kang, J-W. Comparing Graphene Oxide and Reduced Graphene Oxide as Blending Materials for Polysulfone and Polyvinylidene Difluoride Membranes. *Appl. sci.* 2020; **10**:2015.
20. Kizuki, T., Matsushita, T. and Kokubo, T. Apatite-forming PEEK with TiO_2 surface layer coating. *J. Mater. Sci. Mater. Med.* 2015; **26**:5
21. Verdier, T., Coutand, M., Bertron, A. and Roques, C. Antibacterial Activity of TiO_2 Photocatalyst Alone or in Coatings on *E. coli*: The Influence of Methodological Aspects. *Coatings.* 2014; **4**:670-686.
22. Lee, M.J., Kim, M.J., Kwon, J.S., Lee, S.B. and Kim, K.M. Cytotoxicity of Light-Cured Dental Materials according to Different Sample Preparation Methods. *Materials.* 2017; **21**:288-310.
23. Kokubo, T., Kim, H.M. and Kawashita, M. Novel bioactive materials with different mechanical properties. *Biomaterials.* 2003; **24**:2161–2175.
24. Kelly, B.M. *Electrochemical method for characterization and ranking of corrosion inhibitors.* Master thesis. North Dakota State University. 2017.
25. Kokubo, T. and Takadama, H. How useful is SBF in predicting *in vivo* bone bioactivity? *Biomaterials.* 2006; **27**:2907-2915.
26. Awata, M., Okada, M., Takayuki, N. and Matsumoto, N. Improvement of Photocatalytic Activity of TiO_2 Coating by the Modified Sol-gel Method. *Nano Biomed.* 2015; **7**:51-62.
27. Burnat, B., Blaszczyk, T. and Leniart, A. Effects of serum proteins on corrosion behavior of ISO 5832–9 alloy modified by titania coatings. *J Solid State Electrochem.* 2014; **18**:3111–3119.
28. Mokhtari, A., Belhouchet, H. and Guermat, A. In situ high-temperature X-ray diffraction, FT-IR and thermal analysis studies of the reaction between natural hydroxyapatite and aluminum powder. *J Therm Anal Calorim.* 2019; **136**:1515–1526.
29. Ahn, T.K., Lee, D.H., Kim, T.S., Jang, G.C., Choi, S., Oh, J.B. *et al.* Modification of Titanium Implant and Titanium Dioxide for Bone Tissue Engineering. *Adv Exp Med Biol.* 2018; **1077**:355-368.
30. Di Carlo, R., Di Crescenzo, A., Pilato, S., Ventrella, A., Piattelli, A. and Recinella, L. Osteoblastic differentiation on graphene oxide-functionalized titanium surfaces: an *in vitro* study. *Nanomaterials.* 2020; **10**:654.
31. Keshmiri, M. and Troczynski, T. Apatite formation on TiO_2 anatase microspheres. *Journal of J Non Cryst Solids.*, 2003; **3324**:289-294.
32. Gao, P., Li, A., Sun, D.D. and Ng, W.J. Effects of various TiO_2 nanostructures and graphene oxide on photocatalytic activity of TiO_2. *J Hazard Mater.* 2014; **279**:96-104.
33. Zhang, S., Liang, X., Gadd, G.M. and Zhao, Q.I. Advanced titanium dioxide-polytetrafluorethylene (TiO_2-PTFE) nanocomposite coatings on stainless steel surfaces with antibacterial and anti-corrosion properties. *Appl. Surf. Sci.*, 2019; **490**:231–241.
34. Mahé, M., Heintz, J-M., Rödel, J. and Reynders, P. Cracking of titania nanocrystalline coatings. *J. Eur. Ceram. Soc.* 2008; **28**:2003-2010.
35. Almeida, R.M. and Christensen, E.E. Crystallization behavior of SiO_2–TiO_2 sol-gel thin films. *J Sol-Gel Sci Technol.* 1997; **8**:409–413.
36. Hu, M.S., Thouless, M.D. and Evans, A.G., The decohesion of thin films from brittle substrates. *Acta Metall.* 1988; **36**:1301–1307.
37. Zhao, F., Wang, B., Cui, X., Pan, N., Wang, H. and Hou, J. G., Buckle delamination of textured TiO_2 thin films on mica. *Thin Solid Films.* 2005; **489**:221–228.
38. Malnieks, K., Mezinskis, G. and Pavlovska, I. Effect of Different Dip-Coating Techniques on TiO_2 Thin Film Properties. *Key Engineering Materials.* 2016; **721**:128-132.
39. Jalaukan, A.H., Alduwaib, S., Hamed, A., Shohany, B., Etefagh, R. and Khorsand Zak, A. Photocatalytic Activity Antibacterial Effect and Self Cleaning Properties. *Iran. J. Mater. Sci.* 2019; **16**:53-62.
40. Zechner, W., Tangl, S., Fürst, G., *et al.* Osseous healing characteristics of three different implant types: a histologic and histomorphometric study in mini-pigs. *Clin. Oral Implants Res.*, 2003; **14**:150–157.
41. Bousiakou, L.G., Qindeel, R., Al-Dossary, O.M. and Kalkani, H. Synthesis and characterization of graphene oxide (graphene oxide) sheets for pathogen inhibition: *Escherichia coli, Staphylococcus aureus* and *Pseudomonas aeruginosa*, *Journal of King Saud University – Science.* 2022; **34**:102002.
42. Liu, X., Sen, S., Liu, J., Kulaots, I., Geohegan, D., Kane, A., *et al.* Antioxidant deactivation on graphenic nanocarbon surfaces. *Small.* 2011; **7**:2775–2785.
43. Krishnamoorthy, K., Umasuthan, N., Mohan, R., Lee, J. and Kim, S.-J. Antibacterial activity of graphene oxide nanosheets. *Sci. Adv. Mater.* 2012; **4**:1111–1117.
44. Tu, Y., Lv, M., Xiu, P., Huynh, T., Zhang, M., Castelli, M., *et al.* Destructive extraction of phospholipids from *Escherichia coli* membranes by graphene nanosheets. *Nat. Nanotechnol.* 2013; **8**:594–601.
45. Liu, S., Hu, M., Zeng, T.H., Wu, R., Jiang, R., Wei, J., Wang, L., Kong, J. and Chen, Y. Lateral dimension-dependent antibacterial activity of graphene oxide sheets. *Langmuir.* 2012; **28**:12364-12372.
46. Hu, W., Peng, C., Luo, W., Lv, M., Li, X., Li, D., Huang, Q. and Fan, C. Graphene-based antibacterial paper. *ACS Nano.*, 2010; **4**:4317-4323.
47. Ripolles-Avila, C., Martinez-Garcia, M., Hascoët, A-S. and Rodríguez-Jerez, J. Bactericidal efficacy of UV activated TiO_2 nanoparticles against Gram-positive and Gram-negative bacteria on suspension, *CYTA J Food.* 2019; **17**:408-418.
48. Polo, A., Diamanti, M.V., Bjarnsholt, T., Haøiby, N., Villa, F., Pedeferri, M. P. and Cappitelli, F. Effects of photoactivated titanium dioxide nanopowders and coating on planktonic and biofilm growth of *Pseudomonas aeruginosa*. *Photochem. Photobiol.*, 2011; **87**:1387–1394.
49. Zhang, S., Liang, X., Gadd, G.M. and Zhao, Q.I. Advanced titanium dioxide-polytetrafluorethylene (TiO_2-PTFE) nanocomposite coatings on stainless steel surfaces with antibacterial and anti-corrosion properties. *Appl. Surf. Sci.* 2019; **490**:231–241.
50. Zhao, Q., Liu, C., Su, X., Zhang, S., Song, W., Wang, S., Ning, G., Ye, J., Lin, Y. and Gong, W. Antibacterial characteristics of electroless plating Ni–P–TiO_2 coatings, *Appl. Surf. Sci.*, 2013; **274**:101–104.
51. Veltri, S., Palermo, A.M., De Filpo, G. and Xu, F. Subsurface treatment of TiO_2 nanoparticles for limestone: prolonged surface photocatalytic biocidal activities, *Build. Environ.*, 2019; **149**:655–661.
52. Babaei, E., Dehnad, A., Hajizadeh, N., Valizadeh, H. and Reihani, S.F. A study on Inhibitory Effects of Titanium Dioxide Nanoparticles and its Photocatalytic Type on *Staphylococcus aureus*, *Escherichia coli* and *Aspergillus flavus*. *Appl. Food Biotechnol.*, 2016; **3**:115-123.

53. Pan, F., Altenried, S., Zuber, F., Wagner, R.S., Su, Y-H., Rottmar, M., Maniura-Weber, K. and Ren, Q. Photoactivated titanium surface confers time dependent bactericidal activity towards Gram positive and negative bacteria, *Colloids Surf., B*, 2021; **206**:111940.
54. Groves, M.R. and Lucana, D.O. Adaptation to oxidative stress by Gram-positive bacteria: the redox sensing system HbpS-SenS-SenR from *Streptomyces reticuli. Appl Microbiol Microbiotechnol.*, 2010; **1**:33-42.
55. Jiang, W. *Bacterial Toxicity of Oxide Nanoparticles and Their Effects on Bacterial Surface Biomolecules*. 2011. PhD dissertation, University of Massachusetts. Boston, United States.
56. Hočevar, M., Jenko, M., Godec, M. and Drobne, D. An overview of the influence of stainless-steel surface properties on bacterial adhesion. *Materiali in tehnologije.*, 2014; **48**:609-617.
57. Kukhtyn, M., *et al.* Modeling the Process of Microbial Biofilm Formation on Stainless Steel with a Different Surface Roughness. *East. Eur. J. Enterp. Technol.* 2019; **2**:14-21.
58. Guo, S., Kwek, M.Y., Toh, Z.Q., Pranantyo, D., Kang, E.T., Loh, X.J., Zhu, X., Jańczewski, D. and Neoh, K.G. Tailoring Polyelectrolyte Architecture To Promote Cell Growth and Inhibit Bacterial Adhesion. *ACS Appl Mater Interfaces*. 2018; **10**:7882-7891.
59. Tran, T.T.T., Kannoorpatti, K., Padovan, A. and Thennadil, S. A study of bacteria adhesion and microbial corrosion on different stainless steels in environment containing *Desulfovibrio vulgaris. R Soc Open Sci.* 2021; **8**:201577.
60. Stevens, N., Priest, C., Sedev, R. and Ralston, J. Wettability of Photoresponsive Titanium Dioxide Surfaces. *Langmuir*. 2003; **19**:3272–3275.
61. Lee M-K. and Park Y-C. Contact Angle Relaxation and Long-Lasting Hydrophilicity of Sputtered Anatase TiO_2 Thin Films by Novel Quantitative XPS Analysis. *Langmuir*. 2019; **35**:2066–2077.
62. Vrakatseli, V., Farsari, E. and Mataras, D. Wetting Properties of Transparent Anatase/Rutile Mixed Phase Glancing Angle Magnetron Sputtered Nano-TiO_2 Films. *Micro-machines (Basel)*. 2020 ;**11**:616.
63. Yoon, Y., Kye, H., Yang, W.S. and Kang, J-W. Comparing Graphene Oxide and Reduced Graphene Oxide as Blending Materials for Polysulfone and Polyvinylidene Difluoride Membranes. *Appl. Sci.*, 2020; **10**:2015.
64. Shin, Y.C., Bae, J., Lee, J.H., Raja, I.S., Kang, M.S., Kim, B., Hong, S.W., Huh, J. and Han, D. Enhanced osseointegration of dental implants with reduced graphene oxide coating. *Biometar. Res.* 2022; **26**:11.
65. Koenig, S. P., Boddeti, N. G., Dunn, M. L. and Bunch, J. S. Ultrastrong adhesion of graphene membranes. *Nat. Nanotechnol.* 2011; **6**:543–546.
66. Saranya, R., Kavitha, E. and Mohan, D. *Graphene oxide incorporated polyethersulphone membrane for heavy metal ion removal. In: INDA-APDA conference on clean India technologies: role of desalination and water purification*, Chennai, 11–13 February 2016, 61, p. 71. Tamilnadu: INDA-APDA.
67. Cao, X., Wu, K., Wang, C., Guo, Y., Lu, R., Wang, X., *et al.* Graphene Oxide Loaded on TiO_2-Nanotube-Modified Ti Regulates the Behavior of Human Gingival Fibroblasts. *Int J Mol Sci.* 2022; **23**:8723.
68. Sartoretto, S.C., Alves, A.T.N.N., Resende, R.F.B., Calasans-Maia, J., Granjeiro, J.M. and Calasans-Maia, M.D. Early osseointegration driven by the surface chemistry and wettability of dental implants. *J Appl Oral Sci.* 2015; **23**:279–287.
69. Xu, L.C. and Siedlecki, C.A. Effect of surface wettability and contact time on protein adhesion to biomaterial surfaces. *Biomaterials*. 2007; **28**:3273–3283.
70. Yokoi, Y. Osteoblast-like Cell Proliferation, ALP Activity and Photocatalytic Activity on Sintered Anatase and Rutile Titanium Dioxide. *Materials (Basel)*. 2021; **14**:4414.
71. Cervantes, B., López-Huerta, F., Vega, R., Hernández-Torres, J., García-González, L., Salceda, E., Herrera-May, A.L. and Soto, E. Cytotoxicity Evaluation of Anatase and Rutile TiO_2 Thin Films on CHO-K1 Cells *in Vitro. Materials (Basel)*. 2016; **9**:619.
72. Shen, G.X., Chen, Y.C. and Lin, C.J. Corrosion protection of 316 L stainless steel by a TiO_2 nanoparticle coating prepared by sol–gel method. *Thin Solid Films*. 2005; **489**:130-136.
73. Tsou, H.K. and Hsieh, P-Y. Anticorrosive, Antimicrobial, and Bioactive Titanium Dioxide Coating for Surface-modified Purpose on Biomedical Material. 2017. DOI: 10.5772/intechopen.68854.
74. Balamurugan, A., Kannan, S. and Rajeswari, S. Evaluation of TiO_2 coatings obtained using the sol–gel technique on surgical grade type 316L stainless steel in simulated body fluid. *Mater. Lett.*, 2005; **59**:3138-3143.
75. Necolau, M-I. and Pandele, A-M. Recent Advances in Graphene Oxide-Based Anticorrosive Coatings: An Overview. *Coatings*. 2020; **10**:1149.
76. Li, P., Ohtsuki, C., Kokubo, T., Nakanishi, K., Soga, N., Nakamura, T. and Yamamuro, T. *A role of hydrated silica, titania, and alumina in forming biologically active apatite on implant.* In: Transaction of Fourth World Biomaterials Congress. 1992:4.
77. Li, P., Ohtsuki, C., Kokubo, T., Nakanishi, K., Soga, N., Nakamura, T., Yamamuro, T. and de Groot, K. The role of hydrated silica, titania and alumina in inducing apatite on implant. *J Biomed Mater Res.* 1994; **28**:7–15.
78. Londoño-Restrepo, S.M., Jeronimo-Cruz, R., Millán-Malo, B.M., *et al.* Effect of the Nano Crystal Size on the X-ray Diffraction Patterns of Biogenic Hydroxyapatite from Human, Bovine, and Porcine Bones. *Sci Rep*. 2019; **9**:5915.
79. Akin, F.A., Zreiqat, H., Jordan, S., *et al.* Preparation and analysis of macroporous TiO_2 on Ti surfaces for bone-tissue implants. *J Biomed Mater Res.* 2001; **57**:588.
80. Yerokhin, A.L., Nie, X., Leyland, A., *et al.* Plasma electrolysis for surface. *Surf. Coat Technol.*, 1999; **122**:73.
81. Haddow, D.B., James, P.F. and Van Noort, R. Characterisation of sol–gel surfaces for biomedical applications. *J Mater Sci: Mater Med*. 1996; **7**:255–260.
82. Pereira, M.M., Clark, A.E. and Hench, L.L. Effect of texture on the rate of hydroxyapatite formation on gel-silica surface. *J Am Ceram Soc*. 1995; **78**:2463–2468.
83. Dadash, M.S., Karbasi, S., Esfahani, M.N., Ebrahimi, M.R. and Vali, H. Influence of calcinated and non calcinated nanobioglass particles on hardness and bioactivity of sol-gel-derived TiO_2-SiO2 nano composite coatings on stainless steel substrates. *J Mater Sci Mater Med*. 2011; **22**:829-838.
84. Huang, L., Jing, S., Zhuo, O., Meng, X. and Wang, X. Surface Hydrophilicity and Antifungal Properties of TiO_2 Films Coated on a Co-Cr Substrate. *Biomed Res Int.* 2017; **2017**:2054723.
85. Barrère, F., Lebugle, A., Van Blitterswijk, C.A., De Groot, K., Layrolle, P. and Rey, C. Calcium phosphate interactions with titanium oxide and alumina substrates: an XPS study. *J Mater Sci Mater Med*. 2003; **14**:419-425.
86. Lebourg, M. Antón, S. and Gomez Ribelles, J.L. Characterization of calcium phosphate layers grown on polycaprolactone for tissue engineering purposes. *Compos Sci Technol*. 2010; **70**:1796-1804.
87. Li, H., Gong, M., Yang, A., Ma, J., Li, X. and Yan, Y. Degradable biocomposite of nano calcium deficient hydroxyapatite-multi (amino acid) copolymer. *Int J Nanomed*. 2012; **7**:1287-1295
88. Beaufils, S., Rouillon, T., Millet, P., Le Bideau, J., Weiss, P., Chopart, J-P. and Daltin, A-L. Synthesis of calcium-deficient hydroxyapatite nanowires and nanotubes performed by template-assisted electrodeposition. *Mater. Sci. Eng. C.*, 2019; **98**:333-346.
89. Dorozhkin, S.V. A review on the dissolution models of calcium apatites. *Prog Cryst Growth Charact.*, 2002; **44**:45-61.